Journal of Proteomics 211 (2020) 103558

Contents lists available at ScienceDirect

Journal of Proteomics

journal homepage: www.elsevier.com/locate/jprot

ITRAQ-based quantitative proteomic analysis of MG63 in response to HIF-1α inducers

Chunxia Chen, Xuehui Hao, Zhirong Geng*, Zhilin Wang*

State key Laboratory of Coordination Chemistry, School of Chemistry and Chemical Engineering, Collaborative Innovation Center of Advanced Microstructures, Nanjing University, Nanjing 210023, PR China

ARTICLE INFO

Keywords:
Bone fracture
HIF-1α inducers
HIF-1α
iTRAQ
Ca^{2+} /NO/ROS

ABSTRACT

Non-healing fractures constitute a serious clinical problem. HIF-1α is a crucial regulator in response to hypoxia and is proven to be pivotal in bone growth; however, the mechanism still needs further research. In this study, iTRAQ was used to study the effects of two HIF-1α inducers on the expression of proteins in MG63 cells. A total of 841 proteins were significantly changed after treatment with HIF-1α inducers. Among these, 12 proteins were functionally involved in the HIF-1 and VEGF signaling pathways. We then studied the protein and gene expression of the twelve proteins by western blot and RT-PCR, respectively. The results confirmed that VEGF, TFRC, ERK1/2, iNOS, GLUT1, ALDOA, ENO1 and IP3R1 were markedly upregulated, while NF-κB, RCN1, PLCγ1 and CaMKII were significantly downregulated upon treatment with HIF-1α inducers. Meanwhile, the intracellular levels of Ca^{2+}, NO and ROS were closely related and significantly changed. Up-regulation of HIF can maintain high levels of Ca^{2+} and NO while reducing ROS and protect cells from apoptosis induced by low serum. This study presents a new way to study the regulation of HIF on bone growth by investigating the Ca^{2+}, NO and ROS levels.

Signifcance: We found that the regulation of Ca^{2+} and NO proteins are tightly associated with HIF pathway using iTRAQ method. Furthermore, the concentration of Ca^{2+}, NO and ROS are closely related in low serum cultured cells. Up-regulation of HIF pathway can maintain high levels of Ca^{2+} and NO while reducing ROS damage.

1. Introduction

Bone fractures are a familiar condition that often occurs as a result of falls or other accidents. Spine fractures can even take place in everyday activities without any other trauma. Bones possess the postnatal abilities of regeneration and self-repair. However, of the many fractures reported annually in China, there are still many patients who have impaired healing. This results in many patients spending much time and money on treatments, causing a large financial burden to individuals and families. It also has a great impact on social productivity [1]. Therefore, it is very important to investigate the regulatory mechanism of fracture healing. Bone remodeling processes involve the differentiation of osteoblasts and osteoclasts and are regulated by a variety of signaling pathways. For example, Wnt/beta-catenin promotes osteoblasts to differentiate from mesenchymal progenitor cells [2]. The RANKL/RANK/OPG pathway plays an important role in promoting osteoclast differentiation [3]. Activation of the Notch pathway promotes the angiogenesis and osteogenesis of bone [4]. Among the many regulatory pathways, we focused on the hypoxia signaling pathway, as bone is a physiological hypoxic tissue.

HIF is a key regulator in the response to hypoxia and has been confirmed to be activated in fracture healing [5]. HIFs are important transcription factors whose activity is regulated by the hydrolysis of subunits of oxygen-dependent proteins [6]. Under normal oxygen conditions, HIF-1α is constitutively expressed and quickly degraded. The beginning of degradation is the hydroxylation of proline residues by HIF-proline hydroxylase (PHDs). This process requires iron, oxygen and 2-oxoglutarate as cofactors [7]. Under hypoxia, due to the inactivation of PHDs, HIF-1α accumulates and is transferred to the nucleus where it dimerizes with HIF-1β, thereby activating HIF-responsive genes. Small molecule inhibitors of PHDs can block HIF-1α degradation and thus activate the HIF-related pathway; therefore, they can also be called HIF-1α inducers. The molecules that have been studied are mainly iron chelators [e.g., desferrioxamine (DFO)] and 2-oxoglutarate analogues [e.g., dimethyloxalylglycine (DMOG) and L-mimosine (L-mim)], which interfere with the cofactors of the degradation process [8–10]. The HIF pathway regulates many life processes, such as angiogenesis, carbohydrate metabolism and cell proliferation. Especially,

* Corresponding authors.
E-mail addresses: gengzr@nju.edu.cn (Z. Geng), wangzl@nju.edu.cn (Z. Wang).

https://doi.org/10.1016/j.jprot.2019.103558
Received 25 August 2019; Received in revised form 7 October 2019; Accepted 18 October 2019
Available online 23 October 2019
1874-3919/

HIF also plays an important role in the process of fracture healing [11–16].

The initial injury or subsequent treatment of a fracture may lead to insufficient blood supply, a common feature of fracture nonunion. Animal fracture models of nonunion also confirm that nonunion is usually caused by the ablation of vessels and soft tissue at the fracture site [17,18]. In addition, hypovascular or hypoperfusion is observed in most nonunion models (as well as clinical nonunion) [19]. Since the vascular supply is widely recognized as important for tissue and bone repair, research has focused on drug intervention to improve the blood supply in these environments. Vascular endothelial growth factor (VEGF), an important target gene of HIF, has been shown to promote healing of nonunion and critical size defects in rabbits [17,18,20], but it has not successfully increased healing in standard rabbit distraction models [21]. More importantly, because of the need for recombinant protein or gene therapy, the therapeutic application of VEGF may be problematic and expensive. As an alternative approach, we explored the use of small molecules that target the HIF pathway to activate angiogenesis more globally. We hypothesized that HIF activation could be used to increase vascularity in a more generalizable skeletal repair model to heal stabilized femur fractures. However, the regulation mechanisms of the HIF pathway and the target genes involved in fracture healing require further study.

In recent decades, many proteomic platforms for the qualitative and quantitative characterization of protein mixtures and posttranslational modifications have been developed, such as 2D gel-MS [22] and LCMS/MS [23]. At present, iTRAQ stands out from traditional proteomics technologies because of its unique advantages, such as accurate quantification, high-efficiency sample separation, a high identification rate and excellent instrument performance [24]. Moreover, iTRAQ analysis has been further strengthened by powerful bioinformatics tools and statistical analysis [25]. By using the corresponding experimental model and the iTRAQ method, many researchers have made tremendous progress in identifying proteins that are involved in pathogenic processes.

In this study, the effects of two novel PHD inhibitors (IOX2 and FG4592), which are also termed HIF-1α inducers, on the expression of proteins involved in the hypoxia-related signaling pathways in osteosarcoma cell lines were studied. A total of 841 proteins were significantly changed after exposure to the HIF-1α inducers. Among these, 12 proteins were found to be functionally involved in the HIF-1 signaling pathway and the VEGF signaling pathway. Meanwhile, the intracellular levels of Ca^{2+}, NO and ROS were also significantly changed upon treatment with either IOX2 or FG4592. Up-regulation of HIF pathway can maintain high levels of Ca^{2+} and NO while reducing ROS damage. This is a novel finding for HIF-related diseases.

2. Materials and methods

2.1. General

MG63 cells were purchased from the Cell Bank of the Chinese Academy of Sciences. MEM medium, penicillin, streptomycin and fetal bovine serum (FBS) were purchased from Gibco (Gibco, Invitrogen, Calif, USA). All other reagents were of analytical grade and were filtered through a 0.22-μm filter. IOX2 and FG4592 were obtained from SELLECK (Selleck Chemicals, Texas, USA). IOX2 and FG4592 were dissolved in DMSO to form stock solutions and then diluted with culture medium to the indicated concentrations.

2.2. Cell culture

MG63 cells were cultured in MEM medium with 10% FBS in a 5% CO_2 environment at 37 °C. At 90% confluence, the cells were harvested after treatment with 0.25% (*w/v*) trypsin and then re-passaged. Cell growth was observed by a fluorescence microscope (X-Cite® 120PC Q, Lumen Dynamics, Ontario, Canada).

2.3. Cell survival assay

A Cell Counting Kit (Keygen, Nanjing, China) was used to detect the cell viability. MG63 cells were cultured in 96-well plates for 24 h and then various concentrations of IOX2 and FG4592 were added and cultured for another 24 h. To determine cell viability, 10 μL of WST-8 was added to each well. After incubation for 2 h, the absorbance at 450 nm was measured by an automatic enzyme-linked immunosorbent assay plate reader (Thermo Scientific Varioskan Flash, Massachusetts, USA).

2.4. Protein extraction, quantification, digestion and iTRAQ labeling

The MG63 cells were cultured overnight and then pre-incubated with drugs for 24 h. Each sample was then ground into powder in liquid nitrogen and dissolved in a lysis solution [2 M thiourea, 7 M urea, 65 mM DTT, 0.5% Bio-Rad Ampholyte, 4% CHAPS]. The mixture was reacted at 30 °C for 1 h and centrifuged for 20 min at room temperature at 15000*g*. The supernatant after centrifugation was collected and quantified by the Bradford method [26]. A 100 mg aliquot of protein was taken from each sample and dissolved in a buffer solution (AB Sciex, Foster City, CA, USA). The samples were reduced, alkylated and digested with trypsin and then labeled according to the instructions of the iTRAQ Reagents 8-plex kit (AB Sciex). Twenty-four hours later, the samples were collected and labeled with iTRAQ reagents with molecular weights of 113, 114, 115, 116 and 117 Da. After labeling, a strong cation exchange chromatography (SCX) column (Agilent 1200 HPLC; Agilent) was used to collect and purify all samples, and liquid chromatography (LC) with an Eksigent nanoLC-Ultra 2D system (AB Sciex) was used for separation. The LC components were analyzed by a Triple TOF 5600 mass spectrometer (AB Sciex) equipped with a Nanospray III source (AB Sciex, USA) and a pulled quartz tip as the launcher (New Objectives, USA). The data were obtained using 2.5 kV ion spray voltage, 30 PSI curtain gas, 5 PSI spray gas and 150 °C interface heater temperature. For information-dependent acquisition (IDA), survey scans were collected within 250 ms. If the threshold of 150 counts per second (counts/s) was exceeded and the charging state was 2 + to 5 +, up to 35 product ion scans were collected. The total circulation time was fixed at 2.5 s. Rolling collision energy settings were applied to all precursor ions for collision-induced dissociation (CID). The dynamic exclusion peak width K was set to 18 s, and the precursor from the exclusion list was refreshed.

2.5. Protein identification and quantification

The iTRAQ data were processed by Protein Pilot Software v5.0, and the original data were processed according to the MG63 transcription and genome database [27]. Protein identification was carried out with a search option emphasizing biological modifications. The database retrieval parameters were as follows: the instrument was a Triple TOF 5600, iTRAQ quantification, cysteine modified with iodoacetamide, biological modifications were selected as ID focus, with trypsin digestion. To calculate the FDR, an automatic bait database search strategy was used to estimate the FDR by using the Proteomics System Performance Evaluation Pipeline software (PSPEP) that is integrated into the protein testing software. The FDR was calculated by dividing the number of false positive matches by the total number of matches. In the search process, iTRAQ was selected to quantify proteins using unique peptides, and further analysis was carried out considering peptides with fitting values < 1%. In each iTRAQ run, differentially expressed proteins were determined by the ratio of different marker proteins and *p*-values provided by Protein Pilot; the p-values were generated by Protein Pilot using the peptides used to quantify their respective proteins. Finally, for differential expression analysis, the average folding rates at 24 h were 113/117, 114/117, 115/117 and 116/117. Proteins with a

fold change > 1.50 or < 0.67 or a *p*-value < .05 were considered to have significant differences in expression.

2.6. GO and KEGG pathway enrichment analysis

For the GO and KEGG pathway enrichment analysis, all query proteins matching BLASTP were homologously searched according to the *Mus musculus* protein database. The *E*-value was set to $< 1 \times e^{-10}$, and the top 10 best hits for each query sequence were obtained. Of the 10 best hits, those with the best logo for the query were selected as homologous. The GO analysis was carried out via different mapping steps to connect all BLAST hits with the functional information stored in the Gene Ontology database using the DAVID toolkit. Protein IDs and corresponding gene ontology information were linked through public resources such as PIR, NCBI and GO. All comments are associated with the evidence code that provides information about the quality of the functional allocations. For KEGG pathway enrichment analysis, the annotated proteins in the data set were queried in the KEGG database for pathway enrichment, and a protein-protein interaction network was constructed using Cytoscape.

2.7. Determination of intracellular Ca^{2+}

The concentration of intracellular Ca^{2+} in cultured cells was detected by a Ca^{2+} detection kit (Beyotime Institute of Biotechnology, Shanghai, China) after treatment with IOX2 and FG4592 for 24 h, respectively. After incubation with Fluo-3 AM at 37 °C for 35 min, the cells were washed twice with PBS and measured by flow cytometry using BD LSRL Fortessa flow cytometer (Franklin Lakes, NJ, USA). The experimental results were analyzed using FlowJo software (Franklin Lakes, NJ, USA).

2.8. Determination of intracellular NO

The concentration of intracellular NO in cultured cells was determined by a NO detection kit (Beyotime) after treatment with IOX2 and FG4592 for 24 h, respectively. After incubation with DAF-AM at 37 °C for 35 min, the cells were washed twice with PBS and then analyzed by flow cytometry (BD). The experimental results were analyzed using FlowJo software (Franklin Lakes).

2.9. Determination of intracellular ROS

The concentration of intracellular ROS in cultured cells was detected by a ROS detection kit (Beyotime) after treatment with IOX2 and FG4592 for 24 h, respectively. After incubation with DCFH-DA at 37 °C for 30 min, the cells were washed twice with PBS and then measured by flow cytometry (BD). The experimental results were analyzed by FlowJo software (Franklin Lakes).

2.10. Laser confocal microscopy assay

MG63 cells were incubated with corresponding probes (Fluo-3 AM, DAF-AM and DCFH-DA probes of Ca^{2+}, NO and ROS, respectively) at 37 °C for 35 min. The cells were then washed three times with ice-cold PBS and visualized by confocal microscopy (LSM 710, Carl Zeiss, Jena, Germany). Images were acquired using the green channel: λex = 488 nm, λem = 520 nm to monitor the cytosolic fluorescence of Fluo-3 AM, DAF-AM and DCFH-DA probes, respectively. Fluorescence intensity measurements were performed using ZEN 2008 software. For each experiment, cells were monitored at 10-s intervals for a total of 300 s.

2.11. RNA isolation and reverse transcription PCR

Total RNA was extracted according to the instructions provided with TRIzol reagent (Invitrogen). The concentration of each sample was adjusted to two micrograms by using a NanoDrop ND-1000 (Thermo Scientific, USA). Reverse transcription was then performed using a PrimeScript RT-PCR kit. The PCR process used the cDNA as a template and proceeded according to the instructions (TaKaRa Taq™ kit). The number of PCR cycles determined from the plot was 30 for HIF-1α, NOS2, VEGF, P65, TFRC, GLUT1, MAPK1, MAPK3, ENO1, ALDOA, IP3R1, RCN1, PLCγ1 and CaMKIIα and 25 for actin. The amount of amplified product was detected by 1% agarose gel electrophoresis, scanned and analyzed using Quantity One (Bio-Rad, Hercules, CA, USA). The primers are shown in Table S2. Each sample was assayed in triplicate.

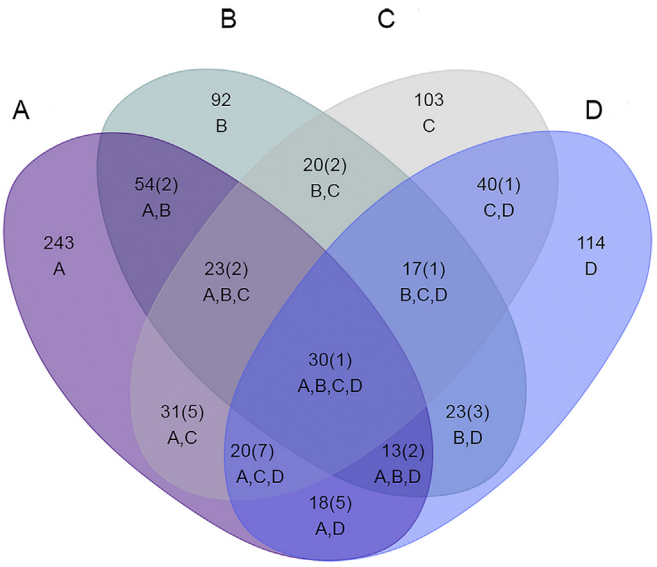

Fig. 1. Changed proteome distribution at different concentrations. Venn diagram showing unique and shared proteins at different concentrations points. A: I30; B: F10; C: F30; D: I10.

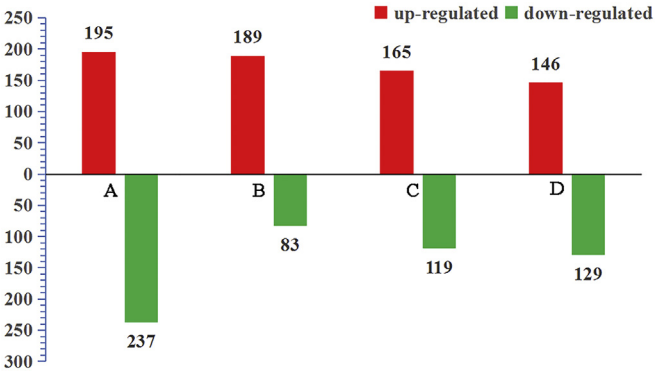

Fig. 2. Number of differentially expressed proteins detected at 24 h. A: I30; B: F10; C: F30; D: I10.

2.12. Western blot analysis

Total protein was collected by protein lysate. The total protein concentration of the sample was determined and adjusted to the appropriate concentration and was then separated by SDS-PAGE (8%–12%). PVDF film was used for transfer. The membrane was blocked for 1 h at room temperature and then incubated with primary antibody at 4 °C overnight. After washing, secondary antibodies were incubated with the membrane for 1 h at room temperature. After washing, enhanced chemiluminescence (ECL, Millipore) photographs were taken.

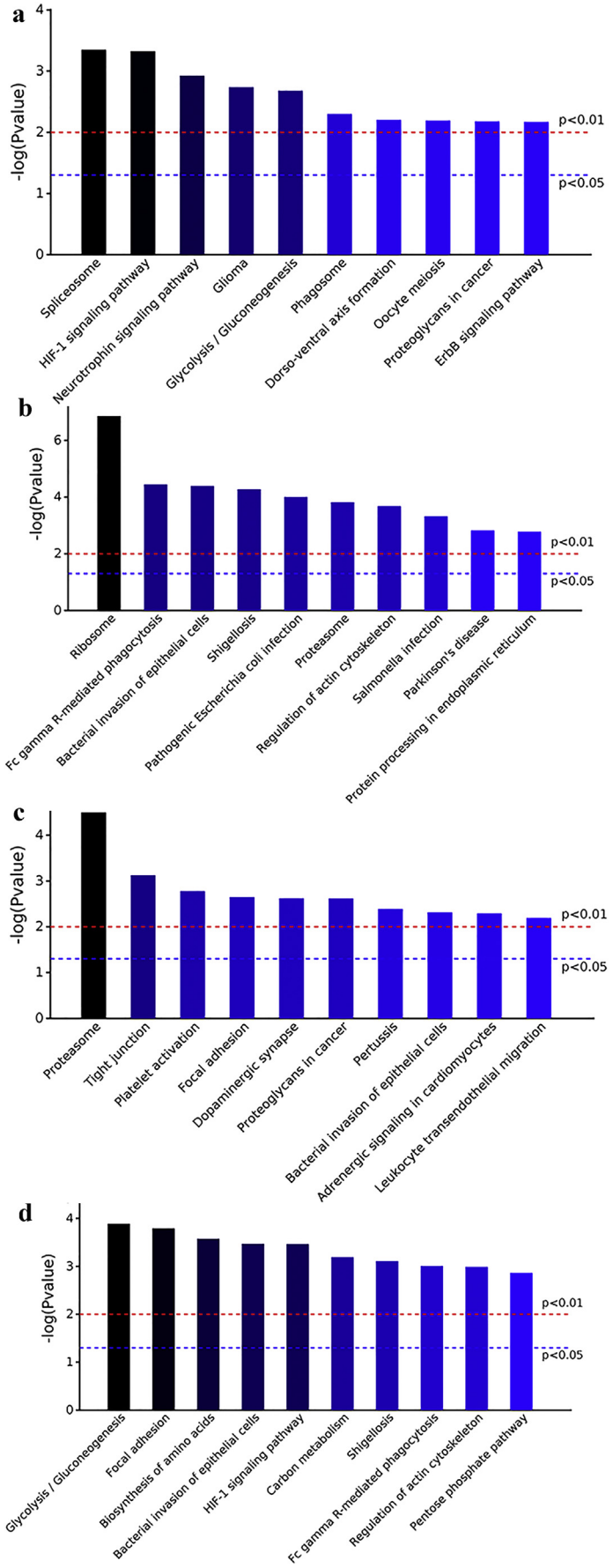

Fig. 3. Most significant KEGG pathways associated with differentially expressed proteins at each concentration point. a: I10; b: I30; c: F10; d: F30.

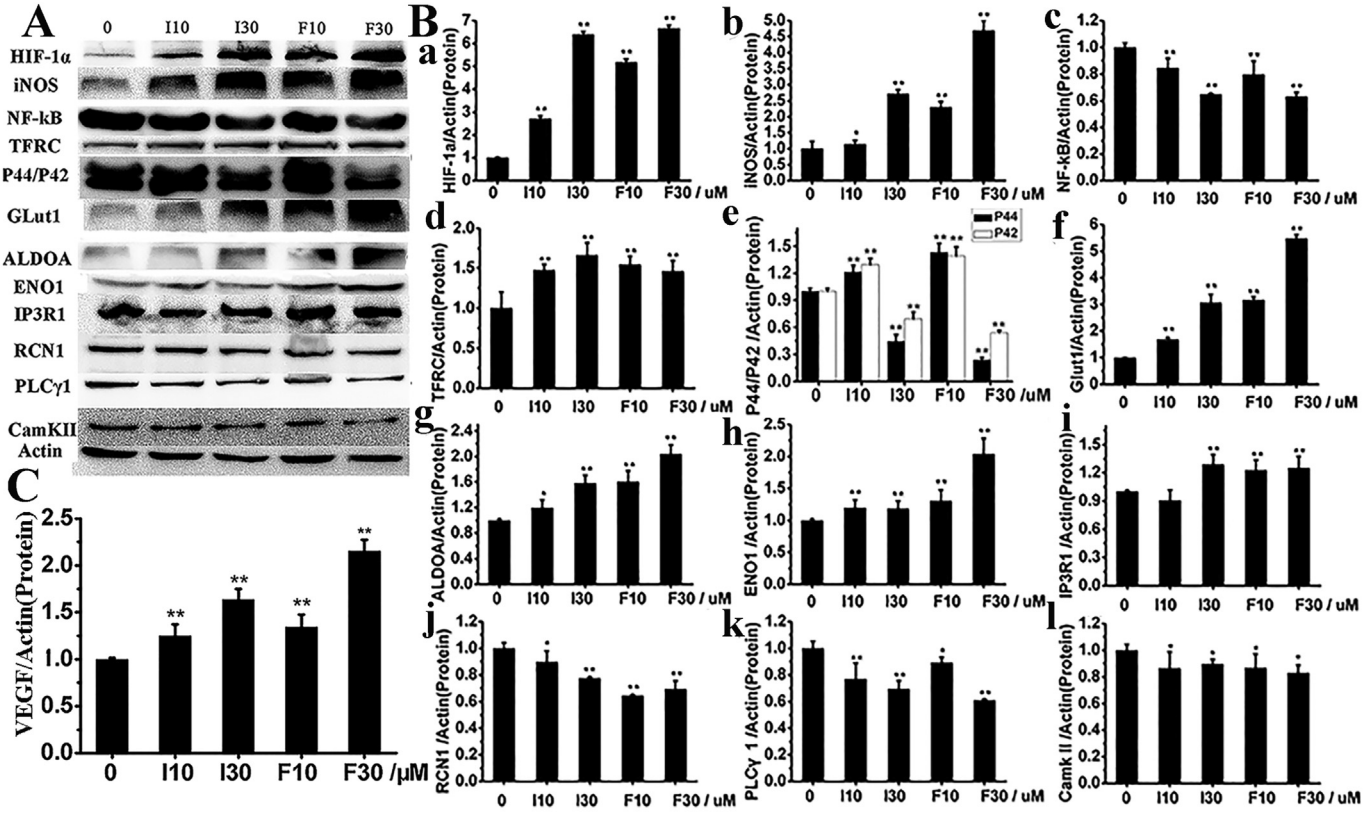

Fig. 4. Effects of IOX2 and FG4592 pre-incubation on protein expression of HIF and related proteins in MG63 cells. (A) Protein expression bands. (B) Statistical analysis of the protein expression levels. (a) iNOS, (b) NF-κB, (c) TFRC, (d) ERK1/2(P44/42), (e) Glut1, (f) ALDOA, (g) ENO1, (h) IP3R1, (i) RCN1, (j) PLCγ1, and (k) CaMKII. (C) Protein expression level of VEGF detected by ELLISA. The protein expression levels are given as the protein/actin ratio. All data in the figures represent the mean value ± SD. *P < 0.05; **P < 0.01.

2.13. ELISA assay

The concentrations of VEGF protein in cultured cells were detected by an ELISA kit (Beyotime) after treatment with IOX2 and FG4592 for 24 h, respectively. The supernatant of the culture medium was collected, and relevant procedures were performed according to the instructions. Protein detection was performed using an automatic ELISA plate reader (Thermo Scientific, Varioskan Flash).

2.14. Cell cycle experiment

MG63 cells were cultured with the given drug concentrations for 24 h. The cells were then collected, fixed with 70% ethanol at 4 °C overnight and stained with propidium iodide (PI). After incubation at 37 °C for 30 min, the cells were washed twice with PBS and then measured by flow cytometry (BD). The experimental results were analyzed by FlowJo software (Franklin Lakes).

2.15. Apoptosis assay

Cells (1×10^6) were collected, washed and resuspended in phosphate buffered saline (PBS), annexin V-fluorescein isothiocyanate (FITC, 5 μL/Tube) and propidium iodide (PI) were added and incubated for 20 min at 37 °C. Cells were analyzed by FACScan flow cytometer (BD) with FlowJo sofware (Franklin Lakes).

2.16. Study on the relationship between Ca^{2+}, NO and ROS in low serum cultured cells

The concentration and correlation of intracellular Ca^{2+}, NO and ROS in low serum cultured cells were also explored. Calcium chelator (BAPTA, 5 μM), NO scavenger (Hb, 5 μM), ROS scavenger (NAC, 5 mM) and H_2O_2 (100 μM) were used to regulate the levels of Ca^{2+}, NO and ROS respectively. The results were collected by laser confocal microscopy.

2.17. Statistical analysis

All tests were repeated three times to ensure reliability of the results. The data are expressed as the mean ± standard deviation (SD). We used one-way ANOVA to compare the differences between two or more independent groups. *P < 0.05 and **P < 0.01 were considered to have statistical significance. IBM SPSS Statistics 20 was used for the statistical analysis.

3. Results

3.1. GO and KEGG analysis of the differential expression proteins

Considering the cytotoxicity tests and the effects of different concentrations of drugs on the accumulation of HIF-1α (Fig. S1, S2), IOX2 and FG4592 (both at 10 μM and 30 μM, named as I10, I30, F10, F30 separately) were selected for subsequent proteomic detection. 3598 distinct proteins were identified and quantified reliably at a global false discovery rate (FDR) of 1%. A total of 841 identified proteins had significant changes in expression levels when the cells were exposed to different drugs and different concentrations compared with the control group, and 30 proteins were differentially expressed at all of the different concentration points (Fig. 1, Table. S1). Among these differentially expressed proteins (DEPs), 432, 272, 284 and 275 up- or down-regulated proteins were identified in the MG63 cells during the short-term IOX2 and FG4592 treatment, respectively (Fig. 2). For an

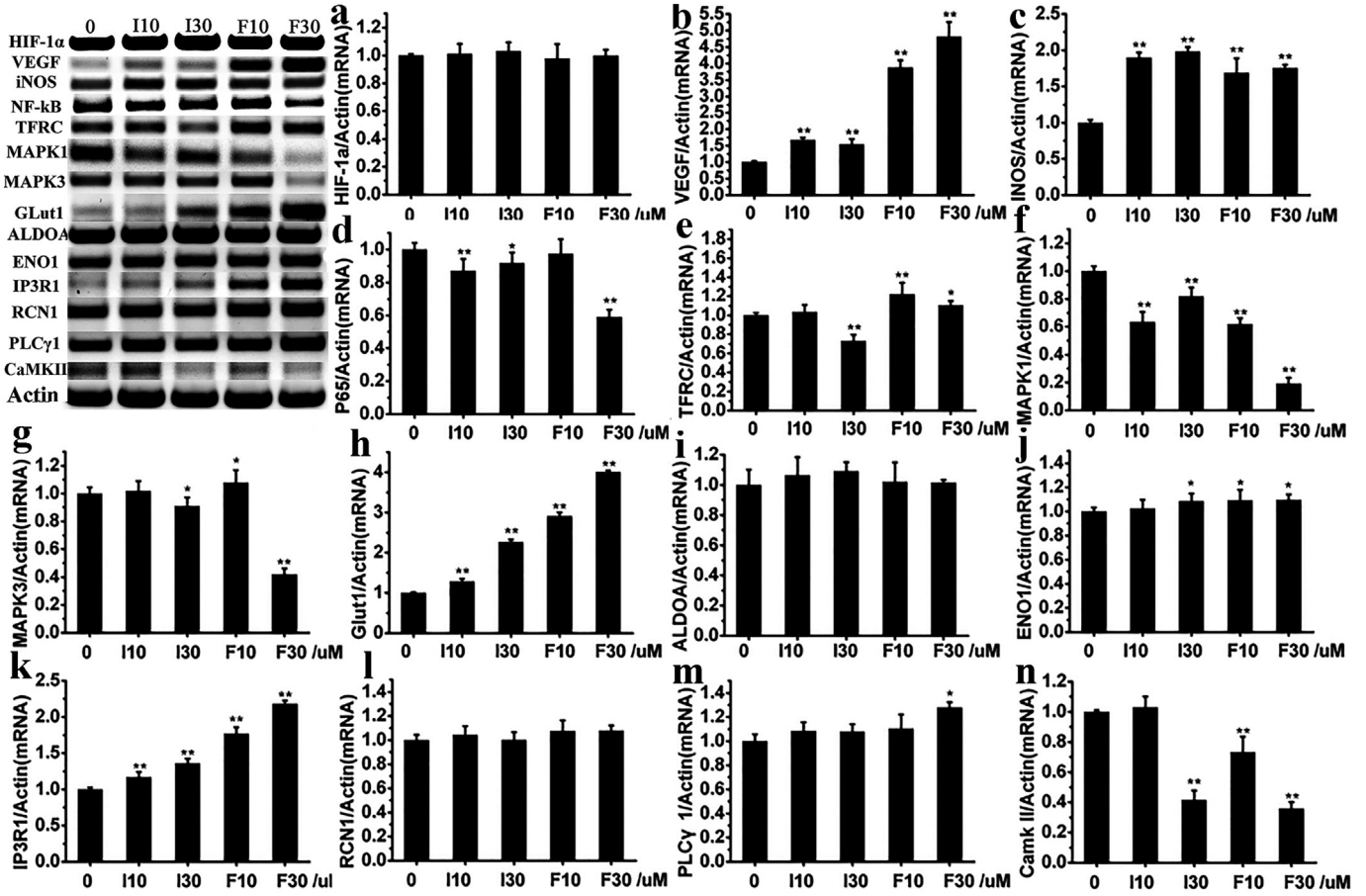

Fig. 5. Effects of IOX2 and FG4592 pre-incubation on mRNA expression of HIF and related genes in MG63 cells. mRNA expression bands and statistical analysis of mRNA expression: (a) *HIF-1α*. (b) *VEGF*. (c) *NOS2*. (d) *NF-κB*. (e) *TFRC*. (f) *MAPK1*. (g) *MAPK3*. (h) *GLut1*. (i) *ALDOA*. (j) *ENO1*. (k) *IP3R1*. (l) *RCN1*. (m) *PLCγ1* and (n) *CaMKII*. The mRNA expressions are given as the mRNA/actin ratio. All data in the figures represent the mean value ± SD. *P < 0.05; **P < 0.01.

overview of the function of all detected DEPs and the potential linkages between them, a GO enrichment analysis was performed for the DEPs detected at each concentration (Fig. S3). The DEPs were classified into the Biological process (BP), Cellular component (CC) and Molecular function (MF) categories. At I30, the DEPs were predominantly binding proteins that were involved in cellular component organization or biogenesis or were involved in the responses to cellular localization. At F10 and F30, the DEPs were also primarily binding proteins that were involved in cellular component organization or biogenesis and in the positive regulation of biological processes. And at I10, the DEPs were predominantly related to the negative regulation of biological processes and to the negative regulation of cellular processes (Fig. 2). Further KEGG pathway enrichment revealed that these proteins were mainly involved in oxidative phosphorylation, carbon metabolism, ribosomes, protein processing in endoplasmic reticulum, regulation of actin cytoskeleton and the VEGF signaling pathway at I30; glycolysis/gluconeogenesis, and the Rap1 signaling pathway, focal adhesion and proteoglycans in cancer at F10; metabolic pathways and the HIF-1 signaling pathway at F30; and metabolic pathways, the HIF-1 signaling pathway and the VEGF signaling pathway at I10 (Fig. 3). The pathways we were interested in for the four concentrations were the HIF-1 signaling pathway and the VEGF signaling pathway, which should be closely related to bone growth and metabolism.

3.2. Protein interaction network

A regulation network was constructed to better understand the relationship between the proteins and affected pathways (Fig. S4). Among them, twelve of the DEPs captured our interest. As shown in the model, p11166 (glucose transporter 1, GLUT1) plays a key role in promoting glucose transport and is encoded by the SLC2A1 gene [28,29]. P04075 (fructose-bisphosphate aldolase A, ALDOA) directly interacts with p09972 (fructose-bisphosphate aldolase C, ALDOC) and p18669 (phosphoglycerate mutase 1, PGAM1) and three glycolysis/gluconeogenesis-related proteins were significantly increased at I10, suggesting an activation of glycolysis upon I10 stimulation. ALDOA is the key enzyme in glycolysis and in the reverse pathway of gluconeogenesis [30]. Therefore, it plays an important role in ATP biosynthesis. P19174 (1-phosphatidylinositol 4,5-bisphosphate phosphodiesterase gamma-1, PLCγ1) catalyzes the formation of inositol 1,4,5-triphosphate and diacylglycerol from phosphatidylinositol 4,5-diphosphate [31]. This reaction uses calcium as a cofactor, so the concentration of calcium ion also affects its activity. Q13554 (calcium/calmodulin-dependent protein kinase type II subunit, CaMKII), which is involved in proteoglycans in cancer, was significantly decreased [32]. CaMKII is a ubiquitously expressed multifunctional serine/threonine kinase that is crucial for Ca^{2+} signal transduction [33]. CaMKII is involved in many signaling cascades and is thought to be an important mediator of learning and memory [34]. P29994 (inositol trisphosphate receptor, IP3R) is a membrane glycoprotein complex acting as a Ca^{2+} channel that is activated by inositol trisphosphate (IP3) [35]. IP3R is not only an important factor in controlling cell division, cell proliferation, apoptosis and other physiological processes [36], it also represents a major second messenger in the process of releasing Ca^{2+} from intracellular storage sites. Many studies have shown that IP3R plays a key role in promoting the transformation of external stimuli into intracellular Ca^{2+} signals. Q15293 (reticulocalbin-1, RCN1) is a calcium-binding protein located in the lumen of the ER. Given that so many calcium-related proteins were

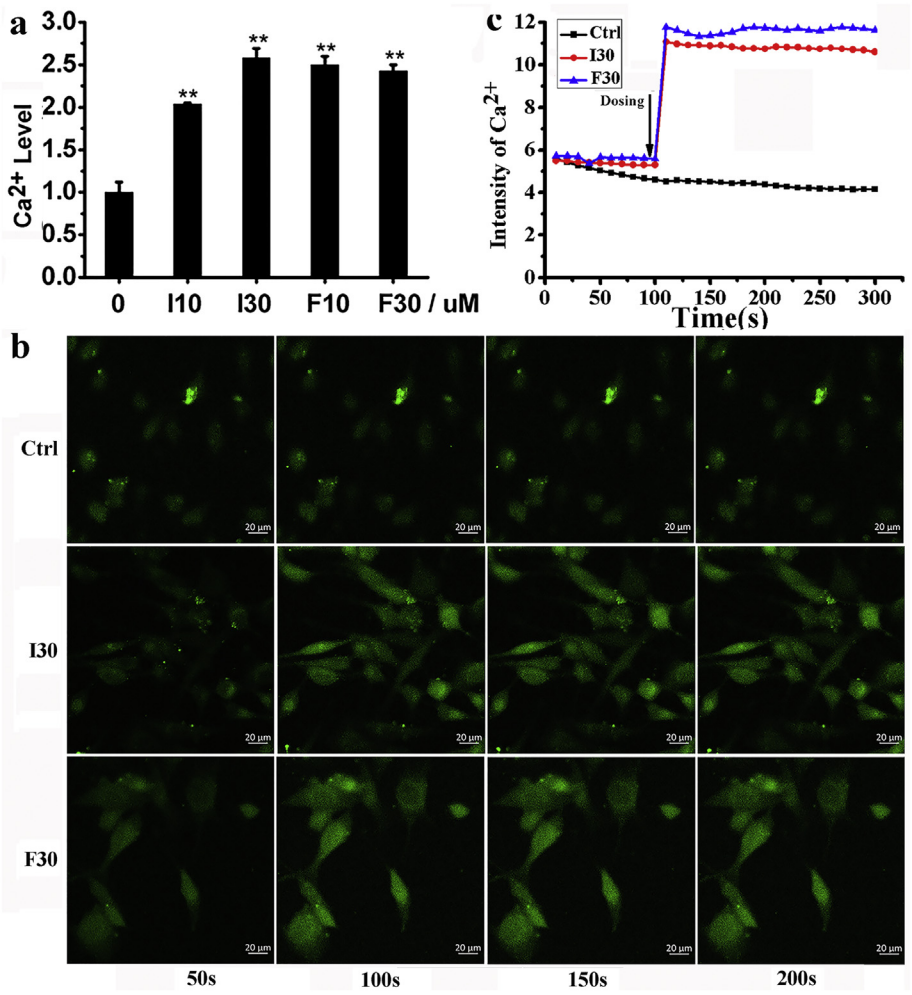

Fig. 6. IOX2 and FG4592 regulate intracellular Ca^{2+}. (a) The intracellular concentration of Ca^{2+} was detected via flow cytometry. (b) Confocal imaging after dosing with IOX2 or FG4592 (30 μM). (c) Quantitative analysis of the fluorescence changes in MG63 cells. All data in the figures represent the mean value ± SD. *P < 0.05; **P < 0.01, compared with the control group. Scale bar: 20 μm.

greatly changed, it was necessary to investigate the relationships between calcium-related pathways and HIF, as well as the Ca^{2+} level [37]. P35228 (inducible nitric oxide synthase, iNOS), also known as nitric oxide synthase 2 (NOS2), produces large quantities of NO upon stimulation; the induction of the high-output iNOS usually occurs in an oxidative environment [38]. Here, the expression of iNOS rose dramatically. The upregulation of Q02750 (dual-specificity mitogen-activated protein kinase kinase 1, MAP2K1) and P28482 (mitogen-activated protein kinase 1, MAPK1) was also notable. The expression and activity of HIF-1α are regulated by various signaling pathways, and extracellular signal-regulated kinase (ERK) is considered to be an effective regulator of HIF-1α expression [39,40]. ERK is a subfamily member of the mitogen-activated protein kinase (MAPK) family, and its pathway has been proven to play an important role in cell survival, growth and proliferation [41]. These are also involved in the neurotrophin signaling pathway. P02786 (transferrin receptor protein 1, TFRC1) can be inhibited by small molecules, leading to growth inhibition [42,43]. P06733 (enolase 1, ENO1) is a glycolytic enzyme expressed in most tissues and plays a role in the oxidative stress of endothelial cells. Both of these proteins were upregulated with HIF activation. Q04206 (transcription factor p65, NF-κB) is part of the NF-κB family of transcriptional activator proteins [44]. The NF-κB and HIF pathways are intimately associated, and there is a significant level of crosstalk between these pathways at a number of levels [45]. It has been reported that HIF-1α can activate NF-κB that NF-κB controls HIF-1α transcription, and that HIF-1α activation may be concurrent with the inhibition of NF-κB [46]. However, the relationship between NF-κB and HIF is still unclear and worth studying. The results of protein-protein interactions were also apparent because the HIF-1α signaling pathway, MEK and ERK were highly upregulated, while NF-κB was downregulated.

3.3. Verification of the HIF-1α pathway related protein expression

To further verificate the HIF-related signaling pathways of MG63 cells treated with IOX2 and FG4592, the protein expression of VEGF, iNOS, NF-κB, TFRC, ERK1/2 (P44/P42), GLUT1, ALDOA, ENO1, IP3R1, RCN1, PLCγ1 and CaMKII were explored by western blot (Fig. 4A). As shown in Fig. 4a, the protein expression of HIF-1α in MG63 cells was elevated in a dose-dependent manner via treatment with either IOX2 or FG4592. TFRC, ERK1/2, iNOS, GLUT1, ALDOA, ENO1 and IP3R1 were upregulated dramatically when treated with IOX2 and FG4592, while NF-κB, RCN1, PLCγ1 and CaMKII were sharply downregulated in a dose-dependent manner (Fig. 4B). The ELISA results showed that IOX2 and FG4592 induced the accumulation of VEGF by 12–200% in a concentration-dependent manner compared with the control group (Fig. 4C).

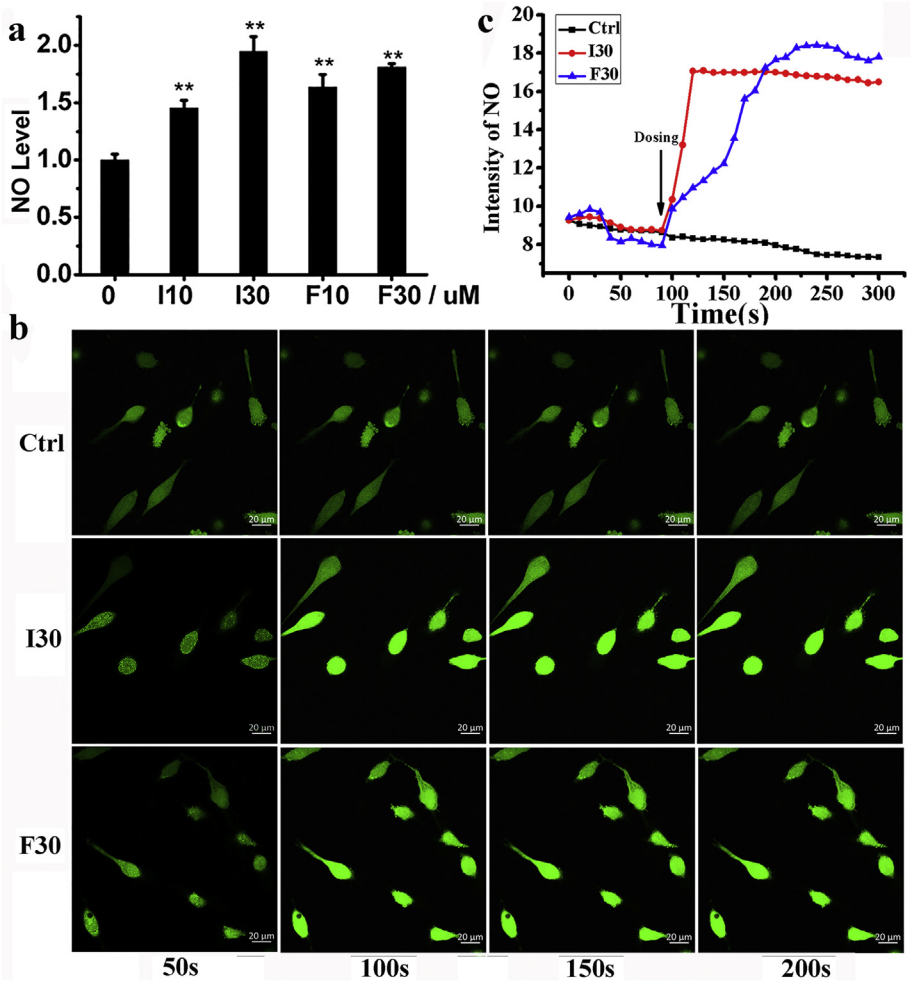

Fig. 7. IOX2 and FG4592 regulate intracellular NO. (a) The intracellular concentration of NO was detected via flow cytometry. (b) Confocal imaging after dosing with IOX2 or FG4592 (30 μM). (c) Quantitative analysis of the fluorescence changes in MG63 cells. All data in the figures represent the mean value ± SD. *P < 0.05; **P < 0.01, compared with the control group. Scale bar: 20 μm.

3.4. Verification of the HIF-1α pathway related mRNA expression

Simultaneously, RT-PCR was employed to analyze the mRNA expression of *HIF-1α*, *VEGF*, *iNOS*, *NF-κB*, *TFRC*, *MAPK1*, *MAPK3*, *GLUT1*, *ALDOA*, *ENO1*, *IP3R1*, *RCN1*, *PLCγ1* and *CaMKII* (Fig. 5). The results showed that the mRNA expression of *HIF-1α*, *ALDOA* and *RCN1* were almost unchanged regardless of preconditioning with either 10 μM or 30 μM IOX2 or FG4592 in MG63 cells. Both IOX2 and FG4592 induced the mRNA accumulation of *VEGF*, *iNOS*, *GLUT1*, *IP3R1* and *ENO1* in a dose-dependent manner compared with the control group. The lower concentration of IOX2 and FG4592 elevated the mRNA expression of *TFRC* and *MAPK3*, but their mRNA expressions were downregulated under high concentrations. *MAPK1* was downregulated at in a dose-dependent manner by preconditioning with IOX2 and FG4592. The results also showed that both IOX2 and FG4592 downregulated mRNA expression of (*NF-κB*) *P65* and *CaMKII* compared with the control group, but the mRNA expression of *PLCγ1* was slightly upregulated with the high dose of FG4592.

3.5. IOX2 and FG4592 regulated intracellular Ca^{2+}

The protein expression profiles indicated that many calcium-related proteins had changed. To explore the role of IOX2 and FG4592 in regard to the Ca^{2+} level, we explored the changes in the intracellular Ca^{2+} level by flow cytometry and confocal microscopy after dosing with IOX2 and FG4592. The intracellular Ca^{2+} level was greatly increased after treatment for 24 h compared with the untreated group (Fig. 6a). Short-term results showed that the intracellular Ca^{2+} concentration rapidly increased after administration and then slowly decreased over time but was maintained at a higher level than the control group (Fig. 6b, c).

3.6. IOX2 and FG4592 regulated intracellular NO

NO is an important factor in regulating blood vessels. We also used flow cytometry and confocal microscopy to detect changes in the NO levels in MG63 cells after dosing. The NO level was also greatly increased after treatment for 24 h (Fig. 7a). Short-term results also showed that intracellular NO concentrations rapidly increased after administration and then slowly decreased over time but were maintained at a higher level than the control group (Fig. 7b, c). These findings were consistent with the changes in calcium.

3.7. IOX2 and FG4592 regulated intracellular ROS

We detected the intracellular ROS level in MG63 cells after treatment with the corresponding concentrations of IOX2 and FG4592. The ROS level was not significantly increased after treatment for 24 h (Fig. 8a). Short-term results also showed that the intracellular ROS concentration rapidly decreased after administration and then slowly decreased until to maintain at a lower level than that of the control group (Fig. 8b, c).

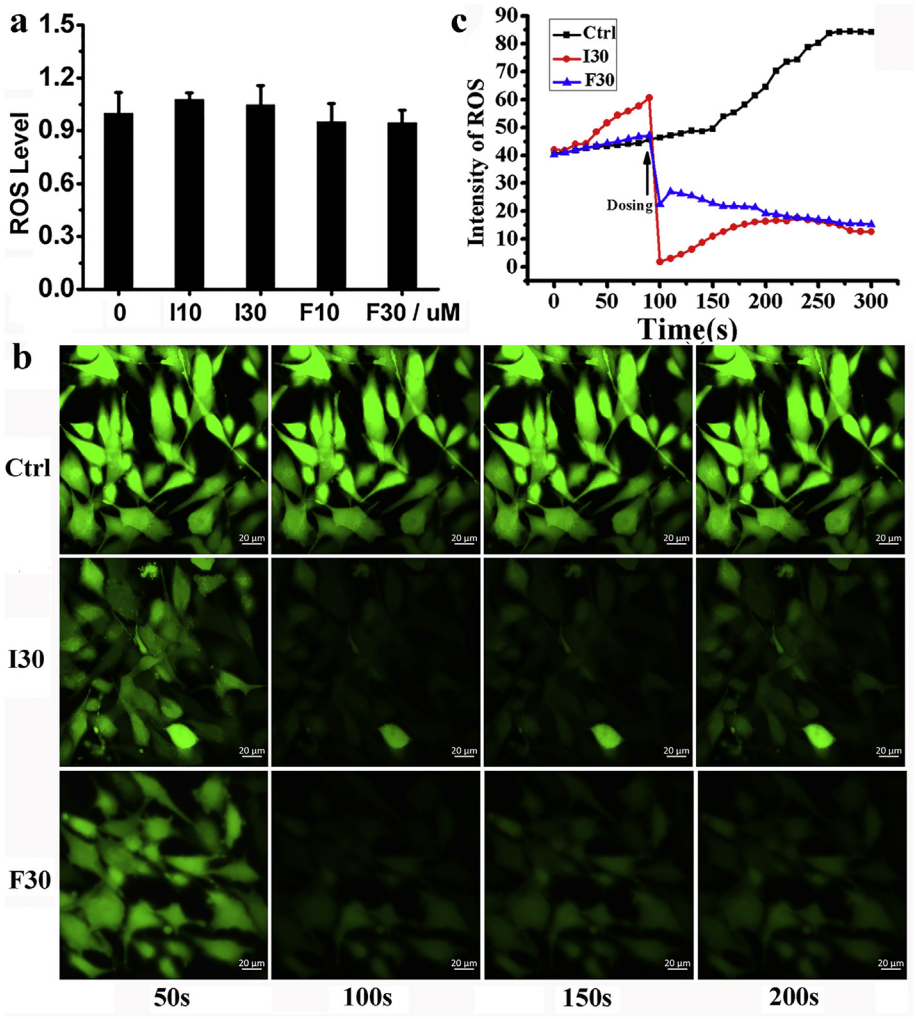

Fig. 8. IOX2 and FG4592 regulate intracellular ROS. (a) The intracellular concentration of ROS was detected via flow cytometry. (b) Confocal imaging after dosing with IOX2 or FG4592 (30 μM). (c) Quantitative analysis of the fluorescence changes in MG63 cells. All data in the figures represent the mean value ± SD. *P < 0.05; **P < 0.01, compared with the control group. Scale bar: 20 μm.

3.8. The concentrations of Ca^{2+}, NO and ROS were closely related in low-serum-cultured cell

Under normal conditions, the intracellular Ca^{2+}, NO and ROS levels are too weak to easy detect by confocal laser scanning microscopy. So we used the low-serum-cultured cells to explore whether the changes of Ca^{2+}, NO and ROS were related. Firstly, we detected the changes of intracellular Ca^{2+}, NO and ROS concentration after treatment for 24 h with 1% FBS respectively. The results showed that (Fig. 9) Ca^{2+}, NO and even ROS levels increased sharply compared with the normal group. Then we used confocal image to detect the changes of fluorescence intensity incubation with Ca^{2+} scavenger (BAPTA), NO scavenger (Hb), ROS scavenger (NAC) or H_2O_2 in 1% FBS medium for 24 h, respectively. As shown in Fig. 9b, the concentration of Ca^{2+} did decrease with the addition of BAPTA, and the level of NO and ROS also decreased. When Hb was added, the fluorescence intensity of NO decreased greatly, and the levels of Ca^{2+} and ROS also decreased. With the addition of ROS scavenger, the ROS level decreased sharply and the levels of Ca^{2+} and NO were also very low. When H_2O_2 was added, the levels of ROS, Ca^{2+} and NO all greatly increased. The results indicated that the concentrations of Ca^{2+}, NO and ROS are closely related. When one changed, the other two responded accordingly.

3.9. IOX2 and FG4592 protected MG63 against low-serum-induced cell apoptosis

In order to investigate the effect of HIF on MG63 cells in in low-serum-medium, we first cultured cells, then transferred the medium to 1% FBS containing drugs for 24 h. The results showed (Fig. 10) that the apoptotic rate of cells was about 20% after 24 h low serum treatment, but very low in the treatment group, which indicated that HIF inducers could protect cells against low serum -induced cell apoptosis.

3.10. IOX2 and FG4592 regulated the cell cycle

We also examined the effect of IOX2 and FG4592 on the cell cycle. The results showed that both small molecules blocked MG63 cells in the S phase (Fig. S5).

4. Discussion

Fracture healing is a complex process that involves many pathways regulating physiological processes, of which HIF plays an important role. To better study the role of HIF in the healing process and the proteins that are regulated, we used a proteomics technology to detect changes in the whole protein expression of MG63 cells after IOX2 or FG4592 treatment. The use of proteomics has provided insights into the

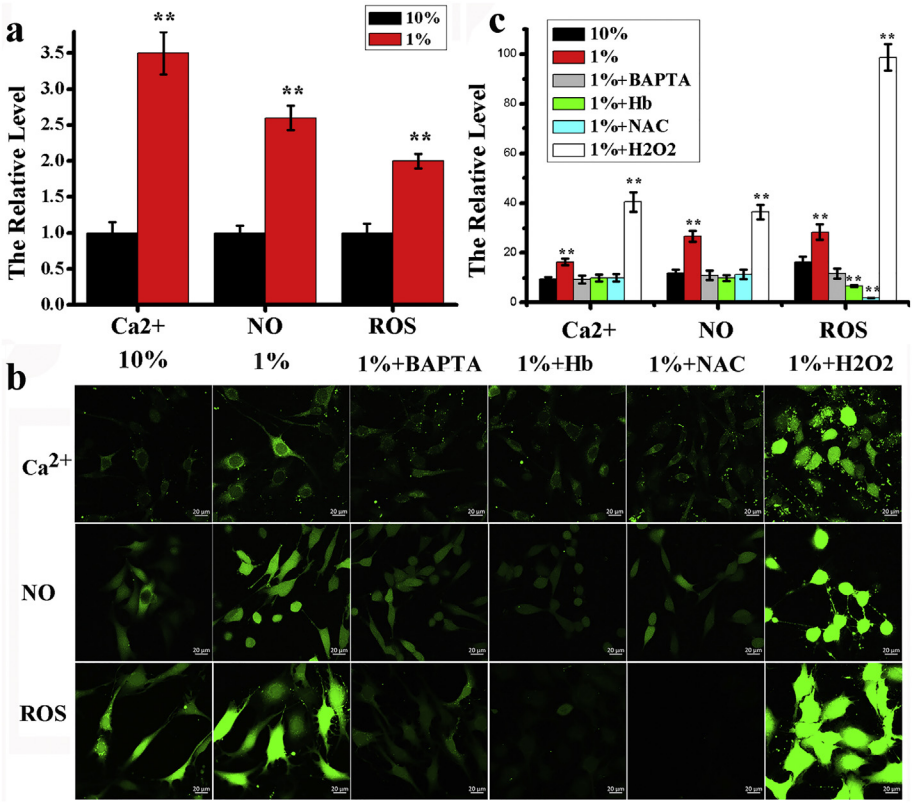

Fig. 9. Changes of Ca^{2+}, NO and ROS concentration in low-serum-cultured cells. (a) The MG63 cells were incubated with 10% FBS (control) or 1% FBS 24 h, the intracellular concentration of Ca^{2+}, NO and ROS were detected via flow cytometry, vs. 10% group. (b) Confocal imaging after incubation with the corresponding experimental conditions: 10% FBS for 24 h, 1% FBS for 24 h, 1% FBS + BAPTA (5 μM), 1% FBS + Hb (5 μM) for 24 h, 1% FBS + NAC (5 mM) for 24 h, 1% FBS + H_2O_2 (100 μM) for 24 h. (c) Quantitative analysis of the fluorescence changes in MG63 cells. All data in the figures represent the mean value ± SD. *P < 0.05; **P < 0.01, compared with the control group. Scale bar: 20 μm.

comprehensive landscape of changes at the molecular level. To explore the core mechanisms, we focused on DEPs. Bioinformatics analyses identified a core connected regulatory network consisting of both upregulated and downregulated proteins. These proteins were functionally involved in the HIF-1, VEGF and Rap1 signaling pathways. The findings suggest that hypoxia and angiogenesis are important reasons for the prognosis of fracture healing. Glycolysis, the neurotrophin signaling pathway and the iron delivery process were also identified in our study, and these processes were connected with the core network, suggesting that they are interlinked with the mechanisms of bone growth. In contrast, the transcription factor p65 was significantly suppressed, leading to abnormal cell growth, which could be a potential mechanism in disturbing the growth and apoptosis function of tissues. We found many proteins with obvious changes that bound to proteins in the interaction network. We validated and confirmed the authenticity of the protein expression by western blot. The proteins included GLUT1, ALDOA, and ENO1, which play an important role in the glycolysis/gluconeogenesis pathways; TFRC and VEGF, which promote erythrocyte production and angiogenesis; iNOS, which induces large quantities of NO production; NF-κB, which plays a regulatory role in inflammatory responses and nuclear transcription; and ERK1/2, RCN1, PLCγ1, CaMKII and IP3R1, which are involved in regulating intracellular Ca^{2+} level.

It is well established that intracellular Ca^{2+} is an important second messenger that plays a key role in regulating numerous cellular activities, e.g., cell proliferation, differentiation, migration, and muscle contraction [47–49]. Physical manipulation of calcium oscillations facilitates osteodifferentiation of human mesenchymal stem cells (hMSCs). Although it is becoming increasingly clear that Ca^{2+} signaling is a regulated mechanism, to our knowledge no study has reported the role of Ca^{2+} regulated by HIF signaling in bone regeneration. As an increasing amount of research effort has recently focused on bone regeneration, studies of the Ca^{2+} oscillations in MG63 cells would be timely. In general, Ca^{2+} signals are mediated by different pathways. Recently published results have indicated that the Ca^{2+} spikes in hMSCs are regulated by the release of Ca^{2+} through IP3R [50], and the application of electrical stimulation is able to couple PLC near the cell surface in human osteoblasts [51]. Signaling studies demonstrate that calcium-sensing receptor (CaSR) stimulation in osteoblasts results in the activation of PLC and ERK1/2 and contributes to osteoblast migration, differentiation and bone remodeling. It also is known that CaM/CaMKII plays a critical role in osteoblastic differentiation [52]. In this regard, our results have shown that a decreased CaMKII protein expression, but the intracellular Ca^{2+} level was significantly increased. Once IOX2 and FG4592 were added, the Ca^{2+} concentration rose immediately (Fig. 6b, c). As time went on, the results remained significant and were consistent with the results of the 24 h treatment. Therefore, we could reasonably speculate that the activator of HIF may increase intracellular Ca^{2+} level by upregulating IP3R1 and ERK1/2. At the same time, Ca^{2+} level is closely related to the HIF pathway. This provided new ideas regarding the role of HIF in bone growth and deserved further study.

NO is a ubiquitous free radical with numerous physiological and pathophysiological roles, and it plays a significant role in bone development both in vitro and in vivo [53,54]. NO is produced through the L-arginine/nitric oxide synthase (NOS) pathway from the terminal guanidino nitrogen of L-arginine [55]. The iNOS-induced production of NO is involved in the inflammatory response in different settings, including acute myocardial infarction [56]. The upregulation of NO expression promotes angiogenesis and improves neurological outcomes after stroke [57]. It has been reported that NO has distinct functional roles depending on the stage of cell differentiation and is a significant tool for bone tissue engineering [58]. Based on these findings, the researchers proposed NO to be involved in coordinating specific phases of osteoblast differentiation and bone formation. However, the regulation mechanisms of the hypoxia signal and NO levels have not been investigated. Experimental results showed that the concentration of NO increased with increasing administered concentration. The NO rose immediately when IOX2 and FG4592 were added (Fig. 7b, c) and remained significant high concentration, which was consistent with the

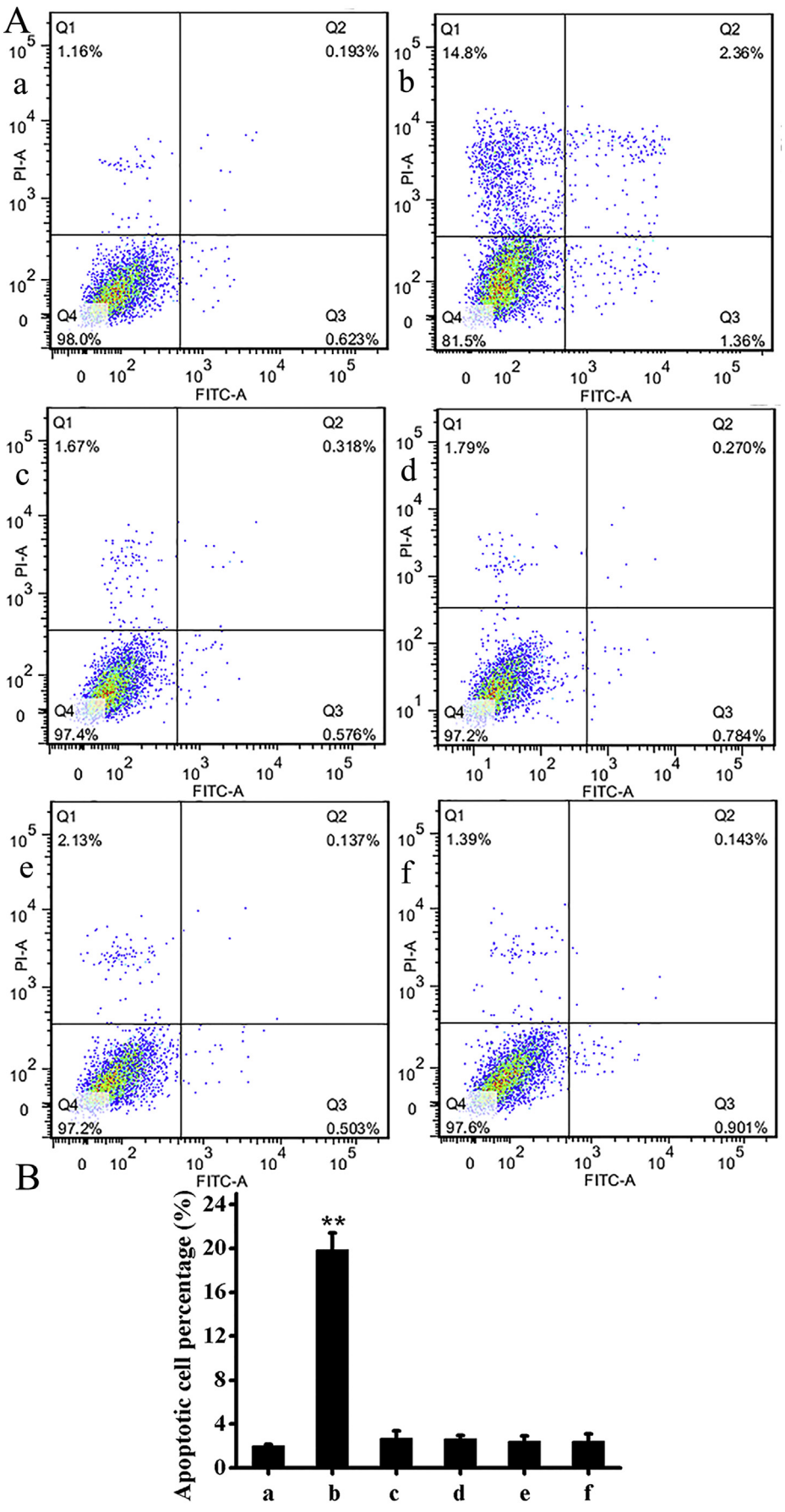

(caption on next page)

Fig. 10. IOX2 and FG4592 protected MG63 against low-serum-induced cell apoptosis. (A) Cell apoptosis was detected by a flow cytometer. The MG63 cells were incubated with (a) 10% FBS (control), (b) 1% FBS, (c) 1% FBS + IOX2 (10 μM) for 24 h, (d) 1% FBS + IOX2 (30 μM) for 24 h, (e) 1% FBS + FG4592 (10 μM) for 24 h, (f) 1% FBS + FG4592 (30 μM) for 24 h. (B) Statistical analysis of the apoptotic cell percentage. The data are presented as mean ± SD of three independent experiments. All data in the figures represent the mean value ± SD., *P < 0.05, **P < 0.01 vs. group (a).

changes of Ca2+.

As a type of free radical, ROS can cause oxidative damage in cells and induce apoptosis. The results found that ROS level did not increase in the cells in 24 h. Confocal microscopy experiments showed that ROS increased slowly without treatment. The ROS level immediately decreased after the IOX2 and FG4592 were added and then continued to be cleared. This suggests that IOX2 and FG4592 might inhibit the production of ROS.

To explore the interaction between Ca^{2+}, NO and ROS, we used the low-serum-cultured cells to text the changes of them. We found that low serum could induce MG63 cells apoptosis. IOX2 and FG4592 could protect MG63 against low serum-induced cell apoptosis. Combining with the levels of Ca^{2+}, NO and ROS, we found that the levels of Ca^{2+}, NO and ROS increased in low serum medium compared with normal group. However, the concentration of Ca^{2+}, NO increased after HIF inducers treatment, the concentration of ROS decreased. Therefore, we could boldly speculate that the apoptosis induced by low serum mainly caused by the increase of ROS. The cell damage caused by elevated concentration of Ca^{2+} and NO was not found in our experiment. When fracture occurs, the increase of Ca^{2+}, NO levels play a critical role in osteoblastic differentiation, cell proliferation, migration [48,49]. Up-regulation of HIF can reduce ROS damage while maintaining high concentration of Ca^{2+}, NO. So it was a very effective way to explore fracture healing process by regulating HIF pathway.

Our results showed that the two drugs promoted the accumulation of HIF and regulated the expression of a series of proteins. Among them, these proteins were related to the intracellular levels of Ca^{2+}, NO and ROS, which would further affect cell metabolism, proliferation and differentiation. Therefore, analyzing the levels of Ca^{2+}, NO and ROS constituted a new way to study the regulatory action of HIF on bone growth. These results provided novel ideas for fracture treatment and deserved further study.

5. Conclusions

A total of 841 proteins were significantly changed after small molecule drug exposure. These proteins were functionally involved in the HIF and VEGF signaling pathways. Glycolysis, the neurotrophin signaling pathway and the iron delivery process were also detected in our study. This work was the first multi-omics study of the basic mechanism of fracture healing, and the results provided a list of potential key regulators of fracture healing in MG63 cells. Pre-incubation with IOX2 and FG4592 stabilized HIF-1α against degradation, thereby stimulating the HIF pathway. Significant changes were observed in VEGF, iNOS, NF-κB, TFRC, ERK1/2, GLUT1, ALDOA, ENO1, IP3R1, RCN1, PLCγ1 and CaMKII proteins expression. And intracellular Ca^{2+} and NO were upregulated, ROS production was inhibited. Moreover, the changes of Ca^{2+}, NO and ROS levels were closely related in low serum cultured cells. Compared with normal culture, 1% FBS resulted in higher apoptotic rate. Upregulation of HIF can reduce apoptosis induced by low serum. This might due to up-regulation of HIF pathway could maintain high levels of Ca^{2+} and NO while reducing ROS damage. Therefore, this study presented a new way to study the regulation of HIF on bone growth by investigating the Ca^{2+}, NO and ROS levels. Therefore, HIF might promote cell survival, cell proliferation, and the cell migration capacity in fracture healing. Additional functional investigations of these proteins could help to elucidate the key targets of fracture healing.

Authors' roles

Study design: CC, ZG and ZW. Study conduct: CC and XH. Data collection: CC. Data analysis: CC. Data interpretation: CC. Drafting manuscript: CC. Revising manuscript content: CC, ZG and ZW. Approving final version of manuscript: ZG and ZW. CC takes responsibility for the integrity of the data analysis.

Declaration of Competing Interest

The authors have no conflicts of interest to disclose.

Acknowledgements

This work is supported by the National Natural Science Foundation of China (21527809, 21775069 and 21976080) and the Six Talent Peaks Project in Jiangsu Province (TD-SWYY-069).

Appendix A. Supplementary data

Supplementary data to this article can be found online at https://doi.org/10.1016/j.jprot.2019.103558.

References

[1] Y. Edward, W. Stuart, K. Toby, The burden of musculoskeletal diseases in the United States, Semin. Arthritis Rheum. 46 (3) (2016) 259–260, https://doi.org/10.1016/j.semarthrit.2016.07.013.
[2] G.J. Spencer, J.C. Utting, S.L. Etheridge, T.R. Arnett, P.G. Genever, Wnt signalling in osteoblasts regulates expression of the receptor activator of NFkB ligand and inhibits osteoclastogenesis in vitro, J. Cell Sci. 119 (2006) 1283–1296, https://doi.org/10.1242/jcs.02883.
[3] K. Sundeep, Minireview: the OPG/RANKL/RANK system, Endocrinology. 142 (12) (2001) 5050–5055, https://doi.org/10.1210/endo.142.12.8536.
[4] S.K. Ramasamy, A.P. Kusumbe, L. Wang, P.H. Adams, Endothelial Notch activity promotes angiogenesis and osteogenesis in bone, Nature. 507 (7492) (2014) 376–380, https://doi.org/10.1038/nature13146.
[5] C. Wan, S.R. Gilbert, Y. Wang, X.M. Cao, X. Shen, G. Rammaswamy, K.A. Jacobsen, Z.S. Alaql, A.W. Eberhardt, L.C. Gerstenfeid, T.A. Einhorn, L.F. Deng, T.L. Clemens, Activation of the hypoxia-inducible factor-1α pathway accelerates bone regeneration, PNAS. 105 (2) (2008) 686–691, https://doi.org/10.1073/pnas.0708474105.
[6] L.E. Huang, J. Gu, M. Schau, H.F. Bunn, Regulation of hypoxia-inducible factor 1α is mediated by an O2-dependent degradation domain via the ubiquitin-proteasome pathway, PNAS. 95 (14) (1998) 7987–7992, https://doi.org/10.1073/pnas.95.14.7987.
[7] M. Ivan, K. Kondo, H. Yang, W. Kim, J. Valiando, M. Ohh, A. Salic, J.M. Asara, W.S. Lane, W.G. Kaelin, HIFa targeted for VHL-mediated destruction by proline hydroxylation: implications for O_2 sensing, Science. 292 (5561) (2001) 464–468, https://doi.org/10.1126/science.1059817.
[8] G.L. Wang, G.L. Semenza, Desferrioxamine induces erythropoietin gene expression and hypoxia-inducible factor1 DNA-binding activity: implications for models of hypoxia signal transduction, Blood. 82 (12) (1993) 3610–3615.
[9] C. Warnecke, W. Griethe, A. Weidemann, J.S. Jurgensen, C. Willam, S. Bachmann, Y. Ivashchenko, I. Wagner, U. Fre, M. Wiesener, K.U. Eckardt, Activation of the hypoxia-inducible factor-pathway and stimulation of angiogenesis by application of prolyl hydroxylase inhibitors, FASEB J. 17 (9) (2003) 1186–1188, https://doi.org/10.1096/fj.02-1062fje.
[10] N.M. Chau, P. Rogers, W. Aherne, V. Carroll, I. Collins, E. McDonald, P. Workman, M. Ashcroft, Identification of novel small molecule inhibitors of hypoxia-inducible factor-1 that differentially block hypoxia-inducible factor-1 activity and hypoxia-inducible factor-1alpha induction in response to hypoxic stress and growth factors, Cancer Res. 65 (11) (2005) 4918–4928, https://doi.org/10.1158/0008-5472.
[11] R.C. Riddle, R. Khatri, E. Schipani, T.L. Clemens, Role of hypoxia-inducible factor-1 alpha in angiogenic osteogenic coupling, J. Mol. Med. 87 (6) (2009) 583–590, https://doi.org/10.1007/s00109-009-0477-9.
[12] D.E. Komatsu, M. Bosch-Marce, G.L. Semenza, M. Hadjiargyrou, Enhanced bone regeneration associated with decreased apoptosis in mice with partial HIF-1α deficiency, JBMR. 22 (2007) 366–374, https://doi.org/10.1359/JBMR.061207.
[13] H.P. Gerber, N. Ferrara, Angiogenesis and bone growth, Trends. Cardiovasc. Med. 10 (5) (2000) 223–228, https://doi.org/10.1016/s1050-1738(00)00074-8.
[14] H. Winet, The role of microvasculature in normal and perturbed bone healing as

revealed by intravital microscopy, Bone. 19 (1) (1996) S39–S57, https://doi.org/10.1016/s8756-3282(96)00133-0.
[15] T.A. Einhorn, J.M. Lane, Angiogenesis in fracture repair, Clin. Orthop. Relat. Res. 355 (1998) S82–S89, https://doi.org/10.1097/00003086-199810001-00010.
[16] M. Nagano, Hypoxia responsive mesenchymal stem cells derived from human umbilical cord blood are effective for bone repair, Stem Cells Dev. 19 (8) (2010) 1195–1210, https://doi.org/10.1089/scd.2009.0447.
[17] H. Eckardt, M. Ding, M. Lind, E.S. Hansen, K.S. Christensen, I. Hvid, Recombinant human vascular endothelial growth factor enhances bone healing in an experimental nonunion model, J. Bone Joint Surg. 87 ((10) (2005) 1434–1438, https://doi.org/10.1302/0301-620X.87B10.16226.
[18] J. Street, M. Bao, L. deGuzman, S. Bunting, F.V. Peale, N. Ferrara, H. Steinmetz, J. Hoeffel, J.L. Cleland, A. Daugherty, N. van Bruggen, H. Paul Redmond, R.A.D. Carano, E.H. Filvaroff, Vascular endothelial growth factor stimulates bone repair by promoting angiogenesis and bone turnover, PNAS. 99 (15) (2002) 9656–9661, https://doi.org/10.1073/pnas.152324099.
[19] M. Murnaghan, G. Li, D.R. Marsh, Nonsteroidal anti-inflammatory drug-induced fracture nonunion: an inhibition of angiogenesis? J. Bone Joint Surg. 88 (Suppl. 3) (2006) 140–147, https://doi.org/10.2106/JBJS.F.00454.
[20] R. Li, D.J. Stewart, H.P. von Schroeder, E.S. Mackinnon, E.H. Schemitsch, Effect of cell based VEGF gene therapy on healing of a segmental bone defect, J. Orthop. Res. 27 (1) (2009) 8–14, https://doi.org/10.1002/jor.20658.
[21] H. Eckardt, K.G. Bundgaard, K.S. Christensen, M. Lind, E.S. Hansen, I. Hvid, Effects of locally applied vascular endothelial growth factor (VEGF) and VEGF-inhibitor to the rabbit tibia during distraction osteogenesis, J. Orthop. Res. 21 (2) (2003) 335–340, https://doi.org/10.1016/S0736-0266(02)00159-6.
[22] T. Rabilloud, M. Chevallet, S. Luche, C. Lelong, Two-dimensional gel electrophoresis in proteomics: past, present and future, J. Proteome 73 (11) (2010) 2064–2077, https://doi.org/10.1016/j.jprot.2010.05.016.
[23] S.S. Thakur, T. Geiger, B. Chatterjee, P. Bandilla, F. Fro¨hlich, J. Cox, M. Mann, Deep and highly sensitive proteome coverage by LC-MS/MS without prefractionation, Mol. Cell. Proteomics 10 (8) (2011), https://doi.org/10.1074/mcp.M110.003699 M110.
[24] C. Evans, J. Noirel, S.Y. Ow, M. Salim, A.G. Pereira-Medrano, N. Couto, J. Pandhal, D. Smith, T.K. Pham, E. Karunakaran, X. Zou, C.A. Biggs, P.C. Wright, An insight into iTRAQ: where do we stand now? Anal. Bioanal. Chem. 404 (4) (2012) 1011–1027, https://doi.org/10.1007/s00216-012-5918-6.
[25] S.M. Herbrich, R.N. Cole, K.P. West, K. Schulze, J.D. Yager, J.D. Groopman, P. Christian, L. Wu, R.N. O'Meally, D.H. May, M.W. Mclntosh, I. Ruczinski, Statistical inference from multiple iTRAQ experiments without using common reference standards, J. Proteome Res. 12 (2) (2013) 594–604, https://doi.org/10.1021/pr300624g.
[26] M.M. Bradford, A rapid and sensitive method for the quantitation of microgram quantities of protein utilizinciple of protein-dye binding, Anal. Biochem. 72 (1–2) (1976) 248–254, https://doi.org/10.1006/abio.1976.9999.
[27] I.V. Shilov, S.L. Seymour, A.A. Patel, A. Loboda, W.H. Tang, S.P. Keating, C.L. Hunter, L.M. Nuwaysir, D.A. Schaeffer, The Paragon Algorithm, a next generation search engine that uses sequence temperature values and feature probabilities to identify peptides from tandem mass spectra, Mol. Cell. Proteomics 6 (9) (2007) 1638–1655, https://doi.org/10.1074/mcp.t600050-mcp200.
[28] A.L. Olson, J.E. Pessin, Structure, function, and regulation of the mammalian facilitative glucose transporter gene family, Annu. Rev. Nutr. 16 (1996) 235–256.
[29] M. Mueckler, C. Caruso, S.A. Baldwin, M. Panico, I. Blench, H.R. Morris, W.J. Allard, G.E. Lienhard, H.F. Lodish, Sequence and structure of a human glucose transporter, Science. 229 (4717) (1985) 941–945, https://doi.org/10.1126/science.3839598.
[30] P. Mamczur, A. Gamian, J. Kolodziej, J. Dziegie, D. Rakus, Nuclear localization of aldolase A correlates with cell proliferation, Biochim. Biophys. Acta 1833 (12) (2013) 2812–2822, https://doi.org/10.1016/j.bbamcr.2013.07.013.
[31] T. Furuichi, S. Yoshikawa, A. Miyawaki, W. Kentaroh, M. Nobuaki, K. Mikoshiba, Primary structure and functional expression of the inositol 1,4,5-trisphosphatebinding protein P400, Nature. 3429 (6245) (1989) 32–38, https://doi.org/10.1038/342032a0.
[32] O. Rokhlin, A.F. Taghiyev, K.U. Bayer, D. Bumcrot, V.E. Kotelianski, R.A. Glover, M.B. Cohen, Calcium/calmodulin-dependent kinase II plays an important role in prostate cancer cell survival, Cancer Biol. Ther. 6 (5) (2007) 732–742, https://doi.org/10.4161/cbt.6.5.3975.
[33] M.J. Berridge, Inositol trisphosphate and calcium signaling, Nature. 36 (1993) 1315–1325, https://doi.org/10.1016/b978-0-12-378630-2.00314-5.
[34] T. Yamauchi, Neuronal Ca^{2+}/calmodulin-dependent protein kinase II—discovery, progress in a quarter of a century, and perspective: implication for learning and memory, Biol. Pharm. Bull. 28 (8) (2005) 1342–1354, https://doi.org/10.1248/bpb.28.1342.
[35] I. Bosanac, J.R. Alattia, T.K. Mal, J. Chan, S. Talarico, F.K. Tong, K.I. Tong, F. Yoshikawa, T. Furuichi, M. Iwai, M. Michikawa, M. Mikoshiba, M. Ikura, Structure of the inositol 1,4,5-trisphosphate receptor binding core in complex with its ligand, Nature. 420 (2002) 696–700, https://doi.org/10.1038/nature01268.
[36] Y. Yoshida, S. Imai, Structure and function of inositol 1, 4, 5-trisphosphate receptor, Jpn. J. Pharmacol. 74 (2) (1997) 125–137, https://doi.org/10.1254/jjp.74.125.
[37] J. Brouwer, I. Roosmalen, B. der Meer, M. Leeuwen, M.D. Posthumus, C. Kallenberg, Expression and regulation of HIF-1 alpha in macrophages under inflammatory conditions; significant reduction of VEGF by CaMKII inhibitor, BMC Musculoskelet. Disord. 11 (2010) 61, https://doi.org/10.1186/1471-2474-11-61.
[38] W.S. Fox, J.T. Chambers, W.J. Chow, Nitric oxide is an early mediator of the increase in bone formation by mechanical stimulation, Am. J. Phys. 270 (6) (1995) 955–960, https://doi.org/10.1152/ajpendo.1996.270.6. e955.
[39] J.H. Lim, E.S. Lee, H.J. You, J.W. Lee, J.W. Park, Y.S. Chun, Ras-dependent induction of HIF-1alpha785 via the Raf/MEK/ERK pathway: a novel mechanism of Ras-mediated tumor promotion, Oncogene. 23 (58) (2004) 9427–9431, https://doi.org/10.1038/sj.onc.1208003.
[40] L. Yuan, M. Santi, E.J. Rushing, R. Cornelison, T.J. MacDonald, ERK activation of p21 activated kinase-1 (Pak1) is critical for medulloblastoma cell migration, Clin. Exp. Metastasis. 27 (7) (2010) 481–491, https://doi.org/10.1007/s10585-010-9337-9.
[41] J. Jin, F. Yuan, M. Shen, Y. Feng, Q. He, Vascular endothelial growth factor regulates primate choroid-retinal endothelial cell proliferation and tube formation through PI3K/Akt and MEK/ERK dependent signaling, Mol. Cell. Biochem. 381 (1–2) (2013) 267–272, https://doi.org/10.1007/s11010-013-1710-y.
[42] M.K. Pandey, B. Sung, K.S. Ahn, A.B. Kunnumakkara, M.M. Chaturvedi, B.B. Aggarwal, Gambogic acid, a novel ligand for transferrin receptor, potentiates TNF-induced apoptosis through modulation of the nuclear factor-Kb signaling pathway, Blood. 110 (10) (2007) 3517–3525, https://doi.org/10.1182/blood-2007-03-079616.
[43] S. Kasibhatla, K.A. Jessen, S. Maliartchouk, J.Y. Wang, N.M. English, J. Drewe, L. Qiu, S.P. Archer, A.E. Ponce, N. Sirisoma, S.C. Jiang, H.Z. Zhang, K.R. Gehlsen, S.X. Cai, D.R. Green, B. Tseng, A role for transferrin receptor in triggering apoptosis when targeted with gambogic acid, PNAS. 102 (34) (2005) 12095–12100, https://doi.org/10.1073/pnas.0406731102.
[44] D. Thanos, T. Maniatis, NF-κB: a lesson in family values, Cell. 80 (4) (1995) 529–532, https://doi.org/10.1016/0092-8674(95)90506-5.
[45] T.Y.H. Lau1, J. Xiao, E.C. Liong, L. Liao, T.M. Leung, A.A. Nanji, M.L. Fung, G.L. Tipoe, Hepatic response to chronic hypoxia in experimental rat model through HIF-1 alpha, activator protein −1 and NF kappa B, Histol, Histopathol. 28 (2013) 463–467.
[46] J. Rius, M. Guma, C. Schachtrup, K. Akassoglou, A.S. Zinkernagel, V. Nizet, R.S. Johnson, G.G. Haddad, M. Karin, NF-κB links innate immunity to the hypoxic response through transcriptional regulation of HIF-1alpha, Nature. 453 (2008) 807–811, https://doi.org/10.1038/nature06905.
[47] S.J. D'Souza, A. Pajak, K. Balazsi, L. Dagnino, Ca^{2+} and BMP-6 signaling regulate E2F during epidermal keratinocyte differentiation, J. Biol. Chem. 276 (26) (2001) 23531–23538, https://doi.org/10.1074/jbc.m100780200.
[48] E. Carafoli, Calcium signaling: a tale for all seasons, Proc. Natl. Acad. Sci. 99 (3) (2002) 1115–1122, https://doi.org/10.1073/pnas.032427999.
[49] R.E. Dolmetsch, U. Pajvani, K. Fife, J.M. Spotts, M.E. Greenberg, Signaling to the nucleus by an L-type calcium channel-calmodulin complex through the MAP kinase pathway, Science. 294 (5541) (2001) 333–339, https://doi.org/10.1126/science.1063395.
[50] S. Kawano, S. Shoji, S. Ichinose, K. Yamagata, M. Tagami, M. Hiraoka, Characterization of Ca^{2+} signaling pathways in human mesenchymal stem cells, Cell Calcium 32 (4) (2002) 165–174, https://doi.org/10.1016/s0143416002001240.
[51] L. Khatib, D.E. Golan, M.R. Cho, Physiologic electrical stimulation provokes intracellular calcium increase mediated by phospholipase C activation in human osteoblasts, FASEB J. 18 (15) (2004) 1903–1905, https://doi.org/10.1096/fj.04-1814fje.
[52] M. Zayzafoon, Calcium/calmodulin signaling controls osteoblast growth and differentiation, J. Cell. Biochem. 97 (1) (2006) 56–70, https://doi.org/10.1002/jcb.20675.
[53] A. Koyama, E. Otsuka, A. Inoue, S. Hirose, H. Hagiwara, Nitric oxide accelerates the ascorbic acid-induced osteoblastic differentiation of mouse stromal ST2 cells by stimulating the production of prostaglandin E2, Eur. J. Pharmacol. 391 (3) (2000) 225–231, https://doi.org/10.1016/S0014-2999(00)00100-X.
[54] J. Aguirre, L. Buttery, M. O'Shaughnessy, F. Afzal, I. de Marticorena, M. Hukkanen, P. Huang, I. MacIntyre, J. Polak, Endothelial nitric oxide synthase gene-deficient mice demonstate marked retardation in postnatal bone formation, reduced bone volume, defects in osteoblast maturation activity, Am. J. Path. 158 (1) (2001) 247–257, https://doi.org/10.1016/S0002-9440(10)63963-6.
[55] S. Moncada, R.M. Palmer, E.A. Higgs, Biosynthesis of nitric oxide from L-arginine: a pathway for the regulation of cell function and communication, Biochem. Pharmacol. 38 (11) (1989) 1709–1715, https://doi.org/10.1016/0006-2952(89)90403-6.
[56] D.A. Ribeiro, J.B. Buttros, C.T. Oshima, C.T. Bergamaschi, R.R. Campos, Ascorbic acid prevents acute myocardial infarction induced by isoproterenol in rats: role of inducible nitric oxide synthase production, J. Mol. Histol. 40 (2) (2009) 99–105, https://doi.org/10.1007/s10735-009-9218-1.
[57] R. Zhang, L. Wang, L. Zhang, Nitric oxide enhances angiogenesis via the synthesis of vascular endothelial growth factor and cGMP after stroke in the rat, Circ. Res. 92 (3) (2003) 308–313, https://doi.org/10.1161/01.res.0000056757.93432.8c.
[58] P.D. DAMOULIS, D.E. DRAKOS, E. GAGARI, D.L. KAPLAN, Osteogenic differentiation of human mesenchymal bone marrow cells in silk scaffolds is regulated by nitric oxide, Ann. N. Y. Acad. Sci. 1117 (1) (2007) 367–376, https://doi.org/10.1196/annals.1402.038.